CrystEngComm

Accepted Manuscript

ROYAL SOCIETY OF CHEMISTRY

www.rsc.org/crystengcomm

Journal Name

RSCPublishing

ARTICLE

Growth and Property Characterization of $CaNdGa_3O_7$ and $SrNdGa_3O_7$ Melilite Single Crystals

Cite this: DOI: 10.1039/xoxxoooooox

Chuanying Shen,[a,b] Shujun Zhang,[b,*] Duanliang Wang,[a] Tianxiang Xu,[a] Haohai Yu,[a] Wenwu Cao,[b] Jiyang Wang,[a] and Huaijin Zhang,[a,*]

Received ooth January 2012,
Accepted ooth January 2012

DOI: 10.1039/xoxxoooooox

www.rsc.org/

Piezoelectric $CaNdGa_3O_7$ and $SrNdGa_3O_7$ single crystals with the melilite structure were successfully grown by the Czochralski technique. Thermal properties of these crystals have been systematically investigated. A full matrix of electromechanical material constants was measured by the IEEE resonance method, with k'_{12} and d_{14} being on the order of 12.5-14.0% and 9.3-9.4 pC/N, respectively. The relationship between physical properties and microstructures was established to explain the anisotropic properties of melilite crystals. In addition, the GaO_4 tetrahedral layers, acting as barriers against charge transport, account for the high electrical resistivity along the *Z*-axis. The high thermal stability of elastic constants and piezoelectric coefficients of $SrNdGa_3O_7$ over the temperature range of 25-600 °C, together with its high resistivity on the order of 9.2×10^6 Ohm·cm at 600 °C, make it a promising candidate for piezoelectric sensing applications at high temperatures.

Introduction

The development of high-temperature piezoelectric sensors has attracted increasing interest in the past few years, particularly in the area of structural health monitoring of aircraft and automobile engines.[1-2] However, candidate materials proposed for high-temperature piezoelectric sensing applications have various shortcomings,[3] for example, the piezoelectric response of α-SiO_2 crystals starts degrading above 350 °C due to the increase of structural disorder,[4] while high conductivity and thermal instability of $LiNbO_3$ limit its usage temperature to less than 600 °C and high frequencies.[5] Although $GaPO_4$ possesses high electrical resistivity and thermal stability of piezoelectric properties up to 950 °C,[6] the high cost of raw materials and small size of achievable crystals limit commercial applications. Despite the good piezoelectric properties of langasite (LGS)-type crystals, the high dielectric loss and low electrical resistivity (less than 10^6 Ohm·cm at 600 °C) limit their high temperature usage.[2] On the other hand, oxyborate crystals exhibit good piezoelectric coefficients, high electrical resistivity and thermal stability, but the monoclinic symmetry and related pyroelectric cross-talk may generate undesirable electrical noise in sensing applications.[2, 7] Thus, new high temperature piezoelectric crystals with simple symmetry, high piezoelectric sensitivity and high thermal stability are desired for high-temperature piezoelectric sensing applications.

It was reported that melilite $Ca_2Al_2SiO_7$ crystals possessed high electrical resistivity of 10^8 Ohm·cm at 800 °C and piezoelectric d_{14} of 6 pC/N,[8-9] drawing our attentions for the exploration of crystals with melilite structures for high temperature piezoelectric applications. Mineral melilites are abundant solid solutions, which were found in igneous and metamorphic rocks, meteorites, and blast furnaceslags.[10] Many melilite-type compounds have been synthesized with a wide range of chemical compositions, including four general formula: $A^1{}_2A^2Z_2O_7$ (A^1=Ca, Sr, Ba, Pb; A^1= Mg, Zn, Cd, Mn, Fe, Co, Cu; Z=Si, Ge); $A^1{}_2X(XZ)O_7$ (A^1=Ca, Sr, Ba; X =Al, Ga; Z=Si, Ge); $(A^1Re)X^1X^2{}_2O_7$ (A^1=Ca, Sr, Ba; Re=rare earth element; X^1 =Fe, Co, Al, Ga; X^2 = Al, Ga) and $(NaA^1)XSi_2O_7$ (A^1=Ca, Sr, Ba; X =Al, Ga).[11] The structure of melilite crystals has tetragonal symmetry with space group of $P\bar{4}2_1m$,[12-13] which was firstly determined by Warren[14] and subsequently refined by Smith[15] and Bindi et al[16]. There are two face shear piezoelectric coefficients d_{14} and d_{36} in melilite crystals with $P\bar{4}2_1m$ symmetry. The piezoelectric coefficient d_{14} of $SrGdGa_3O_7$ was reported to be 14.5 pC/N,[17] much higher than those of quartz (d_{11} =2.3pC/N)[5], $GaPO_4$ (d_{11} =4.5 pC/N)[18] and $La_3Ga_5SiO_{14}$ (d_{11}=6.3pC/N).[19] In this research, large size $CaNdGa_3O_7$ (CNG) and $SrNdGa_3O_7$ (SNG) piezoelectric single crystals were successfully grown by the Czochralski technique. The thermal and piezoelectric properties were systematically investigated. A structure-property relationship was established to explain the anisotropic properties of melilite crystals. In addition, the temperature dependent material properties were measured up to 600 °C, their stability demonstrates the potential usage of these piezoelectric materials at elevated temperatures.

Experimental

Crystal growth and structure analysis

The stoichiometric amounts of raw materials, including high-purity reagents $CaCO_3$ ($SrCO_3$), Nd_2O_3 and Ga_2O_3 powders, were weighed and fully mixed for $CaNdGa_3O_7$ ($SrNdGa_3O_7$) crystal growth. An excess of Ga_2O_3 (1-2% of the total mass) was added to compensate for the evaporation during growth process. The mixtures were calcined at 1000 °C for 10 h to decompose the carbonate, and then ground, mixed, pressed and re-sintered at 1000-1150 °C for 10 h to obtain the polycrystalline compounds. Crystals were grown by the conventional RF-heating Czochralski technique using iridium crucible in an atmosphere of nitrogen containing 2% oxygen by volume. The pressed $CaNdGa_3O_7$ mixtures were melted and kept for 3 hours at a temperature 30 ^oC above the melting point to ensure homogeneity of the melt. A sintered $CaNdGa_3O_7$ polycrystalline bar was used as a seed to pull the $CaNdGa_3O_7$ crystal from the melt with a pulling speed of 0.5-1.0 mm/h and a rotating rate of 10-30 rpm. To avoid cracking caused by the anisotropic thermal stress, the as grown crystal was cooled down to room temperature at a slow rate of 15-25 ^oC/h after the growth process. An [001]-oriented crystal bar with the dimensions of ϕ 4×4 mm^2 (with no obvious scatter pellets and cracking) was cut from the above-grown crystal and used as a new seed to grow high quality single crystals. The growth process of $SrNdGa_3O_7$ is similar to that of $CaNdGa_3O_7$.

The structure of the as-grown crystals was studied by X-ray diffraction (XRD) using crushed powders. The atomic coordinate locations, lattice parameter and bond lengths were determined and refined by Jade 10 software.

The crystals were oriented along the crystallographic directions [002] and [400], by *X*-ray orientation system, from which the crystallographic axes *a*, *b* and *c* can be confirmed. According to the IEEE Piezoelectric,[20] the crystals with space group $P\bar{4}2_1m$ possess physical *X*-, *Y*- and *Z*-axes paralleling to the crystallographic *a*-, *b*- and *c*-axes, respectively.

Thermal property measurements

Thermal properties, including thermal expansion, specific heat, thermal diffusivity and thermal conductivity are important parameters for piezoelectric sensing applications at elevated temperatures. For example, a small divergence of thermal expansion coefficients between the piezoelectric material, electrodes, and package assembly will benefit the sensing with reduced undesired noise and enhanced reliability. The thermal expansion coefficients were measured on specimens with dimensions of 4 × 5 × 6 mm^3 using a thermal dilatometer (Diamond TMA, Perkin-Elmer). The temperature dependent density, which is important for resonance based sensing, such as surface acoustic wave devices, was calculated based on the thermal expansion coefficients. The specific heat was measured by differential scanning calorimetric method in the temperature range of 20-300 ^oC using a simultaneous thermal analyzer (Perkin Elmer Diamond: DSC). The thermal diffusivity was measured along two different crystallographic directions (*X*- and *Z*-) over the temperature range of 30-300 ^oC, from which, the thermal conductivity can be calculated based on equation according to the following formula: $\kappa = \lambda\rho C_p$, where λ is the thermal diffusivity coefficient, ρ is the density, and C_p is the specific heat at constant pressure.

Electromechanical property measurements:

For piezoelectric crystals with $P\bar{4}2_1m$ symmetry, there are 10 nonzero independent electromechanical constants, including two dielectric permittivities, six elastic constants and two piezoelectric coefficients. Different specimens, including transverse extensional bars and face shear plates were made based on the IEEE Standards on Piezoelectricity.[20] Table I lists the specimens, electric field directions together with the corresponding piezoelectric vibration modes for electromechanical constants determination. The dielectric properties were determined from capacitance measured using a high precision LCR meter (Agilent HP 4184A) at 100 Hz - 100 kHz. The elastic constants and electromechanical coupling factors were calculated from the resonance and anti-resonance frequencies of the specimens, which were measured using an Agilent HP 4194A impedance/gain-phase analyzer. The orientation dependent piezoelectric coefficients were calculated by Matlab and Mathematica software. The electrical resistivities were measured using a source meter (Keithley 2410C, Metric Test, Hayward, CA) by the two-probe method. The temperature dependent electromechanical properties were investigated using an Agilent HP 4194A impedance network analyzer, connected to a specially designed sample holder in a high temperature furnace.

TABLE I. Different $CaNdGa_3O_7$ and $SrNdGa_3O_7$ specimens used to measure the electromechanical constants.

Specimens	Dimensions (mm^3)	Electric field Directions	Vibration modes	Material constants
X-plate	8×8×2	*X*	……	ε_{11}
X-plate	8×8×2	*X*	Face shear	s_{44}
Z-plate	8×8×2	*Z*	……	ε_{33}
Z-plate	8×8×2	*Z*	Face shear	s_{66}
(XYt)-5°, *(XYt)*-45°and *(XYt)*-85°	12×4×2	*X*	Length extension	s_{11}, s_{33}, $(2s_{11}+s_{55})$, d_{14}
(ZXt)-45°	12×4×2	*Z*	Length extension	$(2s_{12}+s_{66})$, d_{36}

Results and discussions

Crystal growth and structural analysis

The as-grown $CaNdGa_3O_7$ (melting point 1500 ^oC[22]) and $SrNdGa_3O_7$ single crystals with the size of about ϕ 25×40 mm^3 are shown in Fig. 1. The crystals have no cracks and stacking defects, but a little rough on the surface of $SrNdGa_3O_7$, resulting from the severe evaporation of Ga_2O_3 due to the higher melting point of SNG compared to that of CNG. Fig. 2 shows the XRD patterns, the peaks of the as-grown crystals

match well with the standard card, exhibiting $P\bar{4}2_1m$ space group symmetry.

Fig. 1 The as-grown $CaNdGa_3O_7$ and $SrNdGa_3O_7$ single crystals pulled along [001]-direction.

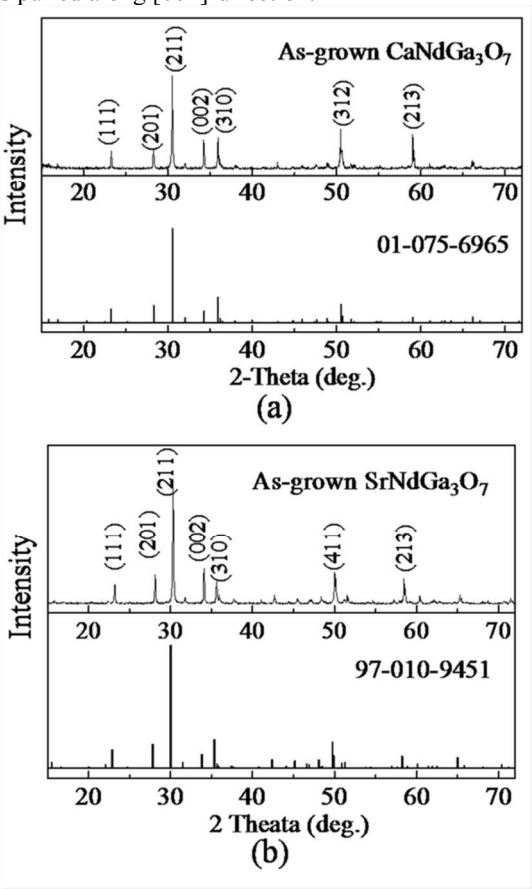

Fig. 2 X-ray powder diffraction (XRD) of $CaNdGa_3O_7$ and $SrNdGa_3O_7$ single crystals.

The structure of $SrNdGa_3O_7$ was analyzed as shown in Fig. 3, which can be described as layers of GaO_4 tetrahedrons (formed in the *XY* plane) alternating along the *Z*-axis, between the layers, Sr^{2+} and Nd^{3+} distributed randomly with a ratio of 1:1 in eight coordinated sites and linked to GaO_4 tetrahedral layers. There are two different types of GaO_4 tetrahedrons and one type of 8-fold SrO_8 (NdO_8) polyhedron. As expected, the structure of $SrNdGa_3O_7$ is almost the same as those of $CaNdGa_3O_7$ and other melilite-type $(A^1Re)X^1X^2{}_2O_7$ crystals.[21-23]

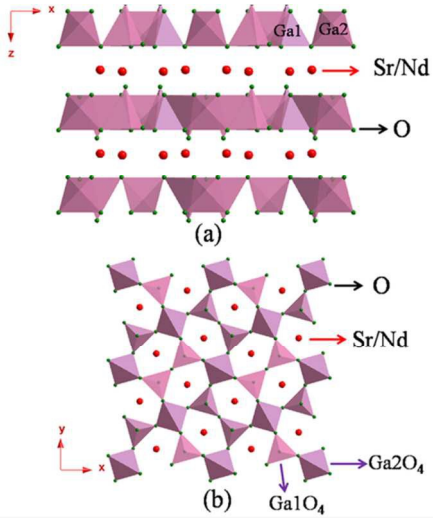

Fig. 3 The structure of $SrNdGa_3O_7$: (a) projected along *Y*-direction; (b) projected along *Z*-direction.

Table II lists the lattice parameters ($a = b$) and bond lengths of Ca-O, Sr-O and Ga-O in $CaNdGa_3O_7$ and $SrNdGa_3O_7$ crystals. From Table II, the bond length of Ca-O is shorter than that of Sr-O, but the ratio of bond length Ca-O to the radius of Ca^{2+} is larger than the bond length Sr-O to the radius of Sr^{2+}, indicating a larger space between the Ca^{2+} and O^{2-} in Ca polyhedrons.

Table II Lattice parameters and bond lengths of Ca-O, Sr-O and Ga-O in $CaNdGa_3O_7$ and $SrNdGa_3O_7$ crystals.

	$CaNdGa_3O_7$ (Å)		$SrNdGa_3O_7$ (Å)	
lattice parameter a	7.90 (1)		8.00(1)	
lattice parameter c	5.23(1)		5.28(1)	
Category of bond	bond lengths		bond lengths	
Ga1-O3(4)	1.83(1)		1.90(1)	
Ga2-O1	1.78(2)		1.80(1)	
Ga2-O2	1.84(2)		1.86(1)	
Ga2-O3(2)	1.76(8)		1.79(1)	
Ca(Sr)1-O1	2.46(1)	Average ratio of Ca-O length to radius of Ca^{2+}: 2.33	2.51(1)	Average ratio of Sr-O length to radius of Sr^{2+}: 2.22
Ca(Sr)1-O2	2.45(6)		2.51(1)	
Ca(Sr)-O3(2)	2.86(1)		2.92(1)	
Ca(Sr)-O2(2)	2.59(3)		2.59(1)	
Ca(Sr)-O3(2)	2.50(1)		2.44(1)	

Thermal properties

Fig. 4 (a) and (b) present the temperature dependence of thermal expansion, exhibiting linear behavior over the studied temperature range of 25-500 °C for both $CaNdGa_3O_7$ and $SrNdGa_3O_7$ crystals. The average thermal expansion coefficients can be calculated from the slope of the curves and were found to be 5.4×10^{-6} /°C and 6.6×10^{-6} /°C along *X*- and *Z*-directions for $CaNdGa_3O_7$ crystals, 5.4×10^{-6} /°C and 6.4×10^{-6} /°C for $SrNdGa_3O_7$ crystals, respectively. Thermal expansion depends on the strength of the chemical bonds along different crystallographic directions. In general, stronger inter-atomic forces associated with lower thermal expansion, while weaker forces relate to higher expansion, accounting for the anisotropic behavior.[24] The small divergence of thermal expansion coefficients along *X*- and *Z*-directions will benefit the selection of electrodes and package assembly easily, thus reduce the undesired noise and enhance sensing package reliability.

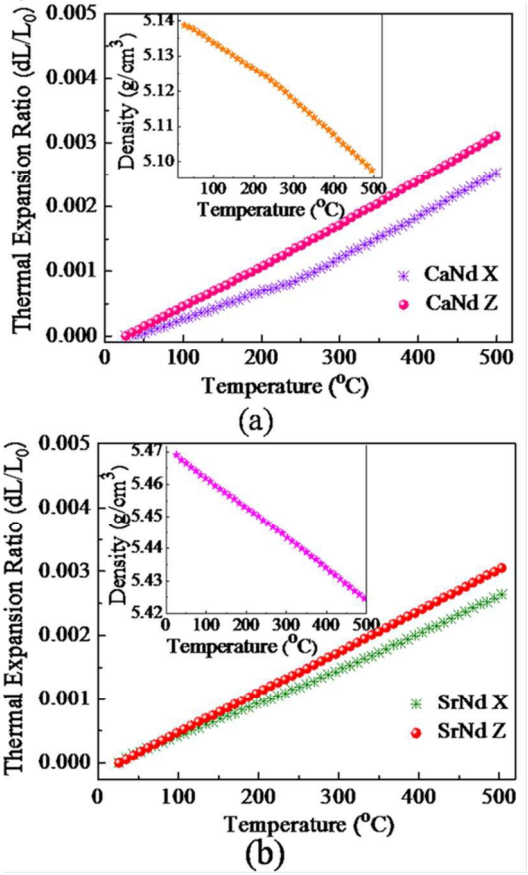

Fig. 4 Thermal expansions of (a) $CaNdGa_3O_7$; and (b) $SrNdGa_3O_7$ as a function of temperature.

The density at different temperatures can be determined according to the following formula:

$$\rho = \frac{m}{abc} = \frac{m}{a_0 b_0 c_0 (1+\frac{\Delta a}{a_0})(1+\frac{\Delta b}{b_0})(1+\frac{\Delta c}{c_0})} = \frac{\rho_0}{(1+\frac{\Delta a}{a_0})(1+\frac{\Delta b}{b_0})(1+\frac{\Delta c}{c_0})} \quad (1)$$

where ρ_0 = 5.14 g/cm^3 and 5.47 g/cm^3 are the room temperature densities measured by Archimedes method for $CaNdGa_3O_7$ and $SrNdGa_3O_7$, respectively; the data of $\Delta a/a_0 = \Delta b/b_0$ and $\Delta c/c_0$ can be obtained from the corresponding thermal expansion curves. As shown in the inset of Fig. 4 (a), the density of $CaNdGa_3O_7$ crystals was found to decrease linearly from 5.14 g/cm^3 to 5.10 g/cm^3, while for $SrNdGa_3O_7$, it decreased linearly from 5.47 g/cm^3 to 5.42 g/cm^3 over the temperature range of 25-500 °C, as observed in the inset of Fig. 4 (b) .

The specific heat as a function of temperature for $CaNdGa_3O_7$ and $SrNdGa_3O_7$ crystals were given in Fig. 5, from which we can see that the specific heat increased slightly with temperature for both crystals. The value of CNG is slightly larger than that of SNG, reaching the same value of 0.60 J/g·°C at 300 °C.

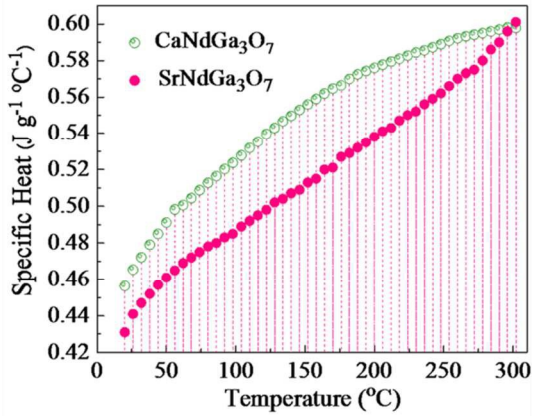

Fig. 5 Specific heats of $CaNdGa_3O_7$ and $SrNdGa_3O_7$ as a function of temperature.

The temperature dependence of thermal diffusion is illustrated in Fig. 6 (a), exhibiting increasing tendency for CNG crystals over the temperature range of 25-300 °C, while SNG maintains similar values along *Z*-direction, with slightly decreased values along *X*-direction. At 25 °C, the thermal diffusions are 0.819 mm^2/s and 0.741 mm^2/s along *X*- and *Z*-axis for CNG crystals; while the values are 0.709 mm^2/s and 0.607 mm^2/s for SNG crystals.

Generally, the thermal conductivity of crystalline materials decreases with increasing temperature, while showing increasing tendency for glasses and alloys.[25] The thermal conductivities of CNG and SNG crystals were found to increase with increasing temperature, showing glasses and/or alloys like behaviors, as given in Fig. 6 (b). The glass and/or alloys like behaviors may relate to their disordered structure.[26-27]

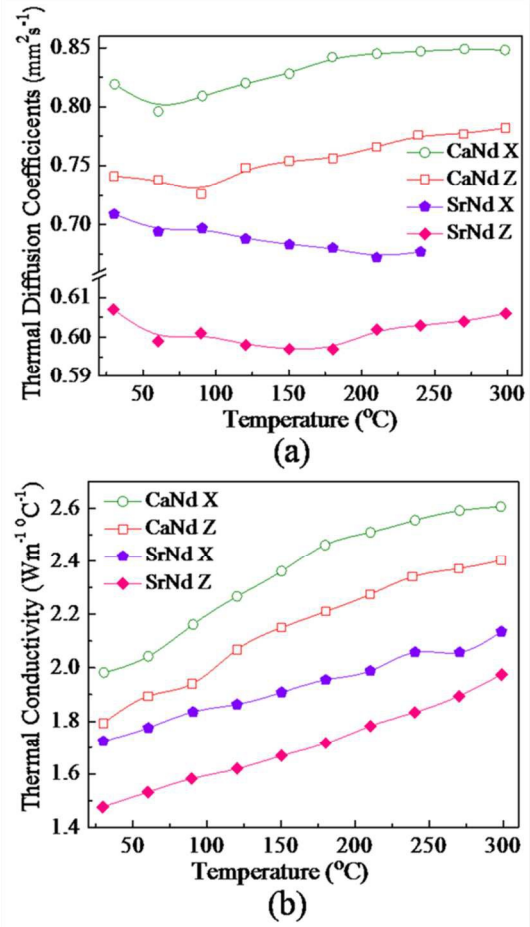

Fig.6 (a) Thermal diffusion; and (b) Thermal conductivity of $CaNdGa_3O_7$ and $SrNdGa_3O_7$ crystals as a function of temperature.

Room temperature electromechanical properties

Table III Room temperature electromechanical material constants of melilite crystals.

	Dielectric Constants ε_{ii}					
	ε_{11}	ε_{33}				
$CaNdGa_3O_7$	16.8	10.9				
$SrNdGa_3O_7$	14.5	9.4				
Crystals	Elastic Compliance Constants s_{ij} (pm^2 /N)					
	s_{11}	s_{12}	s_{13}	s_{33}	s_{44}	s_{66}
$CaNdGa_3O_7$	8.5	-3.5	-1.9	6.8	26.0	16.5
$SrNdGa_3O_7$	7.8	-3.0	-2.7	6.9	25.9	15.9
Crystals	Elastic Stiffness Constants c_{ij} (10^{10} N/m^2)					
	c_{11}	c_{12}	c_{13}	c_{33}	c_{44}	c_{66}
$CaNdGa_3O_7$	16.9	8.5	7.1	18.7	3.8	6.1
$SrNdGa_3O_7$	23.2	14.0	14.6	25.9	3.9	6.3
Crystals	Electromechanical Coupling Factor k_{ij} (%)					
	k'_{12}	k'_{31}	k_{14}	k_{36}		
$CaNdGa_3O_7$	12.5	3.3	15.0	4.2		
$SrNdGa_3O_7$	14.0	3.2	16.3	4.0		
Crystals	Piezoelectric Coefficients d_{ij} (pC/N)					
	d_{14}	d_{36}	d_{11}	d_{15}	d_{26}	
$CaNdGa_3O_7$	9.3	1.7				
$SrNdGa_3O_7$	9.4	1.5				
α-SiO_2	-0.4		2.3			
$GaPO_4$	1.9		4.5			
$La_3Ga_5SiO_{14}$	-6.0		6.2			
$La_3Ta_{0.5}Ga_{5.5}O_{14}$	-3.7		6.6			
$YCa_4O(BO_3)_3$			1.4	7.2	8.0	

Table III lists the full matrix of electromechanical constants at room temperature, in which the dielectric constant ε_{11}, electromechanical coupling factor k_{14} and piezoelectric coefficient d_{14} of CNG and SNG crystals were calculated to be 14.5-16.8, 15-16.3% and 9.3-9.4 pC/N, respectively. The CNG and SNG crystals exhibit good piezoelectric properties when compared with other high temperature piezoelectric crystals, such as α-SiO_2,[5] $GaPO_4$,[5] $La_3Ga_5SiO_{14}$ (LGS),[19] $La_3Ta_{0.5}Ga_{5.5}O_{14}$ (LGT)[28] and $YCa_4O(BO_3)_3$ (YCOB).[29]

As described in the preceding section, both CNG and SNG crystals have the same melilite structure, with GaO_4 layers alternating along the *Z*-axis, between which, Ca^{2+} (Sr^{2+}) and Nd^{3+} distribute randomly with a ratio of 1:1 in eight coordinated sites and linking GaO_4 tetrahedral layers, thus, CNG and SNG possess similar piezoelectric anisotropy behaviors. The large anisotropy in piezoelectric coefficients is associated with the distortion of polyhedrons in crystal structure. Piezoelectric coefficient is a third-rank tensor, i.e., $d_{14} = d_{123}$, $d_{36} = d_{312}$, in which the first subscript number denotes the direction of the applied field, and the other two subscript numbers denote the directions of strain (deformation). With electric field being applied along the *X*- or *Z*-direction, the shear strain S_4 (resulting from the distortion of relatively soft Ca-O, Sr-O polyhedrons in *YZ*-plane) is much larger than S_6 (coming from the distortion of rigid GaO_4 tetrahedrons in *XY*-plane), leading to higher d_{14}. Here, the "soft" and "rigid" mean longer Ca-O/Sr-O bond length (more compressive, thus small c_{44}) and shorter Ga-O bond length (less compressive, thus large c_{66}), respectively.

In addition, a polyhedral model has been successfully used to explain the relationship between the crystal structure and elastic moduli,[30-31] where the elastic moduli are determined by the distortion of polyhedral units. The elastic stiffness constants c_{11} and c_{33} in SNG are larger than those of CNG, being related to the CaO_8 and SrO_8 polyhedrons, which is the only difference in these two crystals. The ratio of Ca-O bond length to Ca^{2+} ion radius is larger than that of Sr-O bond length to Sr^{2+} ion radius, indicating a larger space in Ca polyhedron[32]. Thus, the CaO_8 polyhedron in $CaNdGa_3O_7$ crystals is easier to distort, leading to weaker bond strength, accounts for the smaller values of c_{11} and c_{33} (along physical principal axis) than those of SNG, where the weaker bond strength corresponds to a smaller elastic stiffness[24].

Orientation dependence of piezoelectric coefficient

For $P\bar{4}2_1m$ symmetry, only two face shear piezoelectric coefficients d_{14} and d_{36} exist. Of interest, piezoelectric coefficients d_{12}, d_{13} and d_{33} will appear in the rotated

coordinates. Transverse coefficient d_{12} was investigated with double rotations, where the *XY*-cut samples were first rotated around the *X*-axis for θ then rotated along the *Z*-axis for γ, according to the following formula:

$$d_{12} = d_{14}\cos\theta\sin\theta\cos^3\gamma - (d_{14}+d_{36})\cos\theta\sin\theta\cos\gamma\sin^2\gamma \quad (2)$$

Meanwhile, after a rotation of angle α along the *Z*-axis then rotated β along the *X*-axis for *XZ*- and *XY*-cuts, piezoelectric coefficients d_{13} and d_{33} in the new coordinates can be determined using the following equations:

$$d_{13} = 2d_{14}\cos\alpha\sin\alpha\cos^2\beta\sin\beta - d_{14}(\cos^2\alpha - \sin^2\alpha)\cos\beta\sin^2\beta \quad (3)$$

$$d_{33} = (2d_{14}+d_{36})\cos\alpha\sin\alpha\cos\beta\sin^2\beta \quad (4)$$

Fig. 7 (a), (b) and (c) gives the piezoelectric coefficients as a function of orientations, where the highest d_{12}, d_{13} and d_{33} can be achieved in *XYtw*46°/1°, *XZlt*68°/46°, *ZXtl*46/56°-cut crystals, being on the order of 4.5, 4.7, 3.9 pC/N for $CaNdGa_3O_7$ crystals, 4.4, 4.5 and 3.8 pC/N for $SrNdGa_3O_7$ crystals, respectively. Fig. 7 (d), (e) and (f) illustrates the schematics of the optimized crystal cuts in double rotated coordinates.

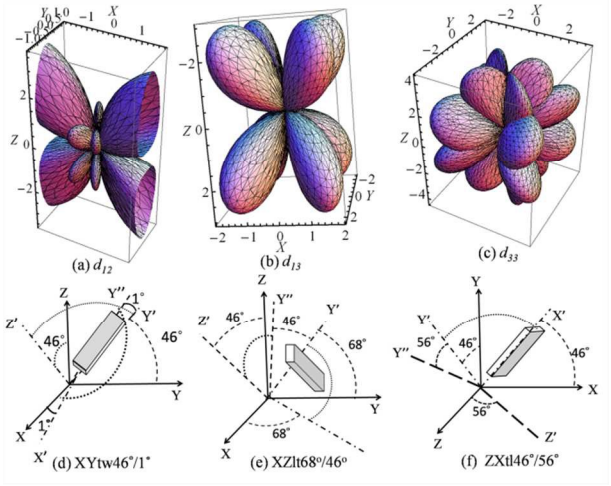

Fig. 7 Orientation dependence of piezoelectric coefficients (a) d_{12}, (b) d_{13} and (c) d_{33}; The schematics of optimized cuts in double rotated coordinates (d) *XYtw*46°/1°, (e) *XZlt*68°/46° and (f) *ZXtl*46/56°-cut specimens.

Temperature dependent electrical resistivity

Fig. 8 shows the electrical resistivity as a function of temperature for melilite crystals and compared with other langasite-type piezoelectric crystals. The activation energies E_a can be calculated from the slopes of the curves and were found to be 1.00 eV and 0.78 eV for *X*- and *Z*-cut $CaNdGa_3O_7$ crystals, 1.08 eV and 0.94 eV for $SrNdGa_3O_7$ crystals, respectively. The activation energy is a phenomenological quantity and expected to reflect defect mobility energy at elevated temperatures.[33] For melilite crystals, the resistivity along the *Z*-direction is more than one order of magnitude higher than the value along the *X*-direction, showing strong anisotropic behavior, due to the layered crystal structure, where the GaO_4 layers consisting of high density interconnected polyhedrons are vertical to the *Z*-direction, acting as barriers against charge transport.[34] In addition, it was reported that a high level of disorder would induce phonon scattering, decreasing the electrical resistivity in disordered langasite-type piezoelectric crystals.[35] Analogous to this, the lower resistivities observed in $CaNdGa_3O_7$ crystals may related to a higher disorder distribution of Ca^{2+} and Nd^{3+} in CNG crystals (due to their similar ionic radii, $r^{Ca}(2+)$ = 1.12 Å, $r^{Nd}(3+)$ = 1.109 Å) than that of SNG ($r^{Sr}(2+)$ = 1.26 Å).[36] In addition, the more evident distortion of GaO_4 tetrahedral layers in $CaNdGa_3O_7$ enables the easier deformation which is a prerequisite deformation for high interstitial oxygen mobility, which may also contribute to the low resistivity of $CaNdGa_3O_7$.[37] Of particular importance is that the resistivity of $SrNdGa_3O_7$ at 600 °C along the *Z*-direction was found to be 9.2 × 10^6 Ohm·cm, higher than those of LGT (1.2 × 10^6 Ohm·cm)[38] and LGS (2 × 10^5 Ohm·cm) crystals.[39]

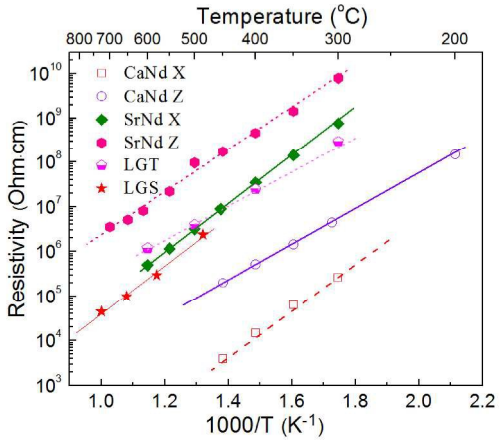

Fig. 8 Electrical resistivity as a function of temperature for high-temperature piezoelectric single crystals.

Temperature dependent dielectric and piezoelectric properties

Fig. 9 presents the dielectric permittivity and dielectric loss, measured at 100 kHz as a function of temperature for CNG and SNG crystals, where the permittivities were found to increase with increasing temperature. When an electric field E_i applied along a physical axis, the induced dipole movement p_i can be calculated based on the formula $p_i = \alpha_i E_i$, where α_i is the polarizability. The difference of dielectric permittivity in CNG and SNG crystals may be induced by the different of Ca^{2+} and Sr^{2+} ions. As discussed previously, the larger ratio of Ca-O bond length to Ca^{2+} ionic radius provides larger space for induced ionic movement,[33] resulting in larger induced dipole moments under applied electric field, so the dielectric permittivities of CNG are expected to be larger than those of SNG crystals. In addition, the dielectric losses were found to increase quickly for CNG over the studied temperature range

(as shown in the inset of Fig. 9), being associated with the increased ionic conduction (low resistivity) at elevated temperatures.

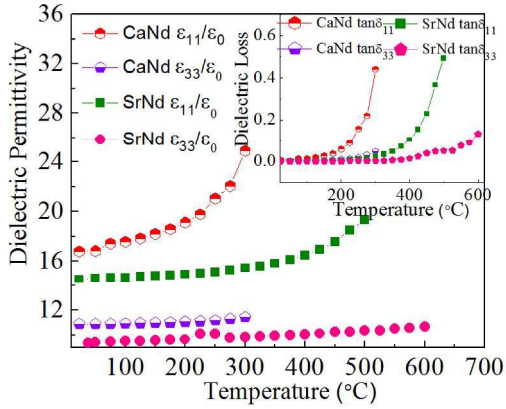

Fig. 9 The dielectric permittivity as a function of temperature for $CaNdGa_3O_7$ and $SrNdGa_3O_7$ crystals.

Knowledge of the temperature dependence of the elastic constants is important for the determination of crystal cuts with zero temperature coefficients of frequency, which are desirable for some types of surface acoustic wave (SAW) devices with frequency stabilization requirements. Elastic constants as a function of temperature for CNG and SNG crystals were investigated, as shown in Fig. 10, from which all the diagonal components of the elastic matrix were found to increase slightly with increasing temperature, with the variation being less than 4% for CNG over the temperature range of 25-300 °C, and less than 3% for SNG over the range of 25-600 °C. For both crystals, the off diagonal components in elastic matrix, s_{12} and s_{13}, were found to show opposite trend, decreased slightly with increasing temperature.

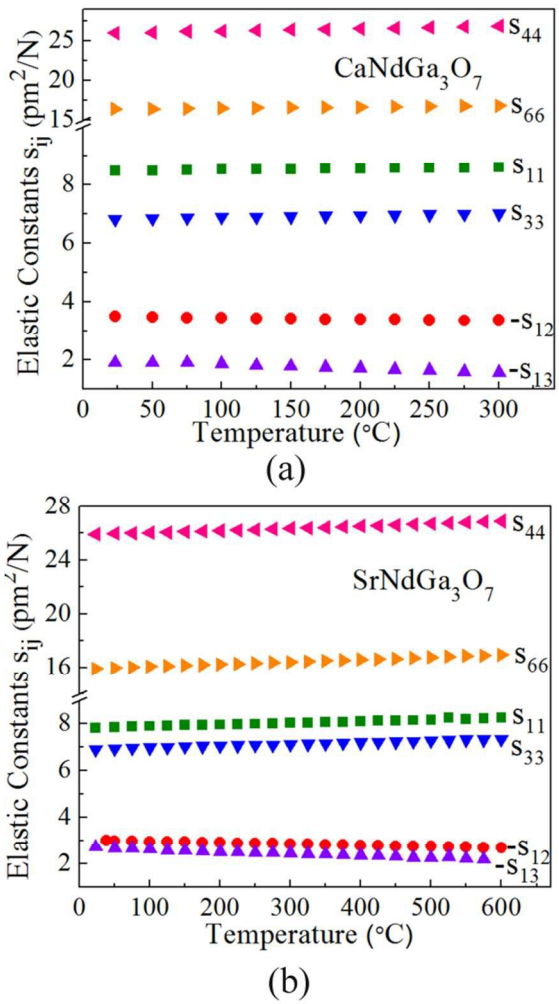

Fig. 10 Elastic constants as a function of temperature for (a) $CaNdGa_3O_7$; (b) $SrNdGa_3O_7$ crystals.

Fig. 11 illustrates the piezoelectric coefficients of (a) $CaNdGa_3O_7$ and (b) $SrNdGa_3O_7$ crystals as a function of temperature. From Fig.11 (a), d_{14} was found to maintain similar values over the temperature range of 25-300 °C, while d_{36} decreased from 1.7 pC/N to 1.1 pC/N. The coupling factors $k_{12}^{'}$ ($XYt/45^o$) and $k_{31}^{'}$ ($ZXt/45^o$) in the 45° rotated coordinates were found to decrease slightly with increasing temperature, as shown in the inset of Fig.11 (a). On the other hand, d_{14} of SNG crystals was found to decrease slightly from 9.4 pC/N to 9.1 pC/N over the temperature range of 25-600 °C, with the overall variation of ~ 3%, showing a high thermal stability. Meanwhile, piezoelectric coefficient d_{36} exhibited a very stable value, as observed in Fig. 11 (b). The inset of Fig. 11 (b) presents the temperature dependence of coupling factors, in which $k_{12}^{'}$ and $k_{31}^{'}$ were found to decrease slightly in the studied temperature range, similar to the tendency observed in CNG. It should be noted that the piezoelectric properties of CNG crystals cannot be measured above 300 °C by resonance method, due to the low resistivity and damping effects to the resonance/anti-resonance frequencies beyond 300 °C.

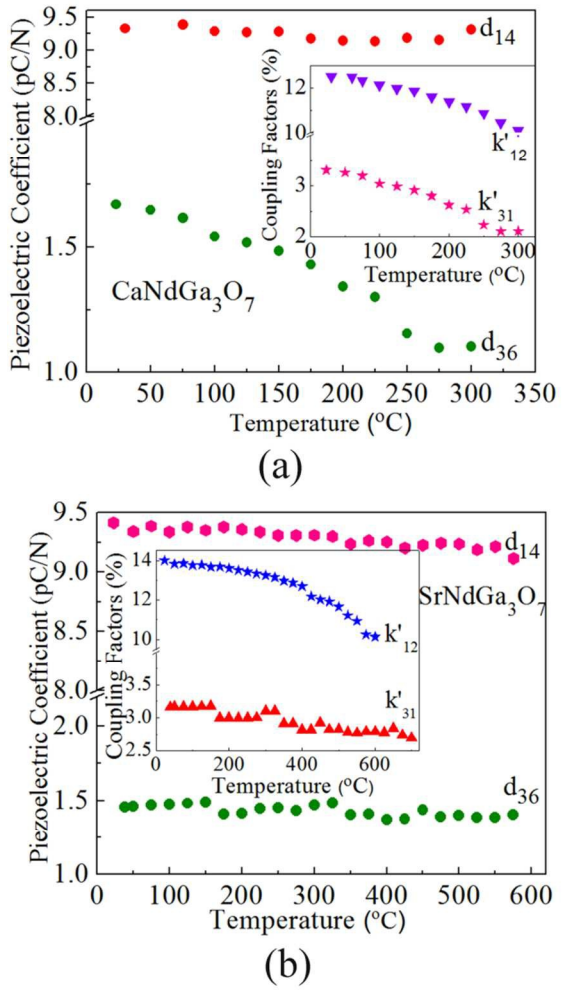

Fig. 11 Piezoelectric coefficients as a function of temperature for (a) $CaNdGa_3O_7$; (b) $SrNdGa_3O_7$ crystals.

Conclusions

$CaNdGa_3O_7$ and $SrNdGa_3O_7$ single crystals with melilite structure were grown using the Czochralski technique. The thermal properties, including thermal expansion, specific heat, thermal diffusivity and thermal conductivity were investigated as a function of temperature, for piezoelectric sensing applications at elevated temperatures. A full matrix of electromechanical constants was determined based on the IEEE resonance method, with k'_{12} and d_{14} being on the order of 12.5-14.0% and 9.3-9.4 pC/N, exhibiting good piezoelectric properties compared to α-SiO_2, LGS, LGT and YCOB piezoelectric crystals. The resistivity of SNG along the *Z*-direction is higher than those of LGT and LGS crystals, due to the GaO_4 tetrahedral layers acting as barriers against charge transport. The high temperature stability of elastic constants is desirable for searching optimum crystal cuts with zero temperature coefficients of frequency. In addition, the high electric resistivity, together with the high thermal stability of piezoelectric coefficient d_{14} for $SrNdGa_3O_7$ over the temperature range of 25-600 °C, make it a good candidate for piezoelectric sensing applications at high temperatures.

Acknowledgements

The authors would like to thank Prof. Thomas R. Shrout for helpful discussions; the author C. Shen wants to thank Hengjang Cong for the crystal growth and the Chinese Scholarship Council for the support of oversea studies.

Notes and references

[a]State Key Laboratory of Crystal Materials, Institute of Crystal Materials, Shandong University, Jinan, Shandong 250100, China. E-mail: huaijinzhang@sdu.edu.cn
[b]Materials Research Institute, Pennsylvania State University, University Park, Pennsylvania 16802, USA. E-mail: soz1@psu.edu

†Electronic Supplementary Information (ESI) available: [details of any supplementary information available should be included here]. See DOI: 10.1039/b000000x/

1 X. Jiang, K. Kim, S. Zhang, J. Johnson and G. Salazar, *Sensors*, 2004, 14, 144-169.
2 S. J. Zhang, F. P. Yu, *J. Am. Ceram. Soc.*, 2011, 94,
3 D. Damjanovic, Curr. Opin. *Solid State Mater. Sci.*,1998, 3, 469-473.3153–3170.
4 J. Haines, O. Cambon, D. A. Keen, M. G. Tucker and M. T. Dove, *Appl. Phys. Lett.*, 2002, 81, 2968-2970.
5 R. C. Turner, P. A. Fuierer, R. E. Newnham and T. R.Shrout, *Applied Acoustics*,1994, 41, 299-324.
6 T. R. Shrout, R. Eitel, and C. A. Randall, in *Piezoelectric Materials in Devices*, edited by N. Setter (EPFL Swiss Federal Institute of Technology, Switzerland, 2002), p. 413.
7 F. P. Yu, S. Hou, S. J. Zhang, Q. M. Lu, and X. Zhao, *Phys. Status Solidi A*, 2014, 211, 574 (6 pages).
8 H.Takeda, M. Hagiwara, H. Noguchi, T. Hoshina, T. Takahashi, *Appl. Phys. Lett.*, 2013,102, 242907 (4 pages).
9 M. Hiroaki, H. Noguchi, T. Hoshina, H. Takeda, S. Fujihara, N. Kodama and T. Tsurumi, *Jpn. J. Appl. Phys*, 2013, 52, pp. 09KD03.
10 W. A. Deer, R. A. Howie and J. Zussman, An introduction to the rock-forming minerals, 2nd edn, Longman, London (1992).
11 A. A. Kaminskii, L. Bohat´y,P. Becker, J. Liebertz, P. Held, H.J. Eichler, H. Rhee,and J. Hanuza, *Laser Phys. Lett.* 2008, 5, 845–868.
12 Y. I. Sigalovskaya, Y. Z. Nozik, and A. B. Tovbis, *Sov. Phys. Crystallogr.* 1989, 34, 185-189.
13 S. F. Bartram, *Acta Crystallogr. B*1967, 25, 791-795.
14 B. E. Warren, *Z Kristallogr*, 1930, 74, 131-138.
15 J. V. Smith, *Am Mineral,* 1953, 38, 643-661.
16 L. Bindi, P. Bonazzi, M. Dusek, V. Petricek and G. Chapuis, *Acta Crystallogr (B)* 2001, 57,739-746.
17 Y. Y. Zhang, X. Yin, H. H. Yu, H. J. Cong, H. J. Zhang, J. Y. Wang and R. I. Boughton, *Cryst. Growth Des*, 2011, 12, 622-628.
18 P. Krempl, G. Schleinzer and W. Wallnöfer. *Sensors and Actuator*, 1997, 61, 361-363.
19 S. J. Zhang, Y. Q. Zheng, H. K. Kong, J. Xin, E. Frantz, and T. R. Shrout, *J. Appl. Phys.*, 2009,105, 114107.
20 IEEE Standard on Piezoelectricity, ANSI/IEEE Std 176-1987 (American Standards National Institute, New York, 1987).

21 A. A. Kanwski, E. L. Beloeonev, B. V. Mili,S. E. Sarkiso, and K. Kurbano, *phys. stat. sol.*,1986, 97, 279-290.
22 S. Kubota, M. Izumi, H. Yamane, M. Shimada, *J. Alloys Compd.*, 1999, 283, 95–101.
23 W. Ryba-Romanowski, S. Gołab, J. Hanuza and M. Berkowski, *J. Phys. Chem. Solids*, 1989, 50, 685-692.
24 R. E. Newnham, Properties of Materials: Anisotropy, Symmetry and Structure (Oxford University, London, UK, 2005).
25 C. Kittel, *Phys. Rev.*, 1949, 75, 972-974.
26 Y. Y. Zhang, H. J. Zhang, H. H. Yu, J. Y. Wang, W. L. Gao, M. Xu, S. Q. Sun, M. H. Jiang, and R. I. Boughton, *J. Appl. Phys.*, 2010, 108, 063534 (10 pages).
27 Y. Y. Zhang, H. J. Zhang, H. H. Yu, S.Q. Sun, J. Y. Wang, and M. H. Jiang, (28) *IEEE J Quantum Elect*, 2011, 47, 1506-1513.
28 J. Bohm, E. Chilla, C. Flannery, H.-J. Fröhlich, T. Hauke, R. B. Heimaann, M. Hengst, U. Straube, *J.Cryst. Growth*, 2000, 216, 293-298.
29 H. Shimizu, T. Nishida, H. Takeda, T. Shiosaki, *J. Cryst. Growth*, 2009, 311, 916–920.
30 D. J. Weidner, J. D. Bass, M. T. Vaughan, In: Akimoto S, Manghnani M (eds) High-pressure research ingeophysics. Center for Academic Publications, 1982, 125-133.
31 Z. Li, S.K. Chan, and S. Ghose. *Phys Chem Minerals*, 1990, 17, 462-466.
32 F. P. Yu, S. J. Zhang, X. Zhao, S.Y. Guo, X. L. Duan, D.R. Yuan and T. R Shrout. *J. Phys. D: Appl. Phys.*, 2011, 44,135405 (6 pages).
33 S. J. Zhang, Y. Q. Zheng, H. K. Kong, J. Xin, E. Frantz, and T. R. Shrout, *J. Appl. Phys.*, 2009, 105, 114107 (6 pages).
34 M. Miyayama, I.S. Yi. *Ceram. Int.*, 2000, 26, 529-533.
35 B. H. T. Chai, A. N. P. Bustamante, and M. Chou, "A new class of ordered langasite structure compounds," in *IEEE Int. Frequency Control Symp.*, 2000, 163-168.
36 R. D. Shannon, *Acta Crystallogr., Sect. A*, 1976, 32, 751-767.
37 F. X. Wei, T. Baikie, T. An, M. Schreyer, C. Kloc, and T. J. White, *JACS*, 2013, 133, 15200-15211.
38 H. Takeda, J. I. Yamaura, T. Hoshina, and T. Tsurumi, *J. Ceram. Soc. Jpn.*, 2010, 118, 706.
39 S. J. Zhang, H. K. Kong, R. Xia, Y. Q. Zheng, J. Xin, and T. R. Shrout, *Solid State Commun.*, 2010,150, 435-438.

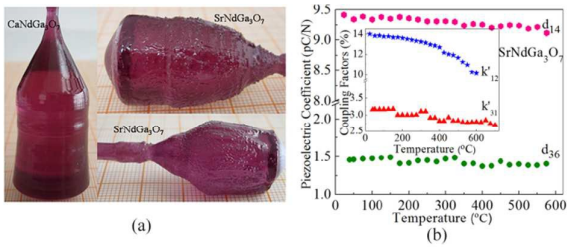

Large size $CaNdGa_3O_7$ and $SrNdGa_3O_7$ single crystals grown along [001] direction and Piezoelectric coefficients for $SrNdGa_3O_7$ as a function of temperature.